THE JOURNAL OF NAVIGATION (2020), **73**, 892–911.
doi:10.1017/S0373463320000028

Improved Semi-Bit Differential Acquisition Method for Navigation Bit Sign Transition and Code Doppler Compensation in Weak Signal Environment

M. Nezhadshahbodaghi, M. R. Mosavi and N. Rahemi

(*Department of Electrical Engineering, Iran University of Science and Technology, Narmak, Tehran 16846-13114, Iran*)
(E-mail: M_Mosavi@iust.ac.ir)

The presence of code Doppler and navigation bit sign transitions means that the acquisition of global positioning system (GPS) signals is difficult in weak signal environments where the output signal-to-noise ratio (SNR) is significantly reduced. Post-correlation techniques are typically utilised to solve these problems. Despite the advantages of these techniques, the post-correlation techniques suffer from problems caused by the code Doppler and the navigation bit sign transitions. We present an improved semi-bit differential acquisition method which can improve the code Doppler and the bit sign transition issues in the post-correlation techniques. In order to overcome the phenomenon of navigation bit sign transitions, the proposed method utilises the properties of the navigation bit. Since each navigation bit takes as long as 20 ms, there would be 10 ms correlations duration integration time between the received signal and the local coarse/acquisition (C/A) code in which the navigation bit sign transitions will not occur. Consequently, this problem can be cancelled by performing 10 ms correlations in even and odd units separately. Compensation of the code Doppler is also accomplished by shifting the code phase of the correlation results. To validate the performance of our suggested method, simulations are performed based on three data sets. The results show that the quantity of required input SNR to detect at least four satellites in the proposed method is −48·3 dB, compared with −20 dB and −9 dB, respectively, in traditional differential and non-coherent methods.

KEYWORDS

1. GPS. 2. Weak Signal. 3. Post-Correlation Techniques. 4. Code Doppler. 5. Bit Sign Transition.

Submitted: 21 February 2019. Accepted: 23 December 2019. First published online: 11 February 2020.

1. INTRODUCTION. Because of the application of global satellite navigation systems (GNSS) in various dimensions of industry, urban canyon, military and extensive scientific research, they are considered among the essential technologies of today's world.

Satellite-based navigation systems are able to estimate the receiver position, velocity and time (PVT) information in real-time. Global Positioning System (GPS), which is widely used in military and civilian domains, is the most common GNSS (Kaplan and Hegarty, 2005). In a software receiver, the digitised signals enter into the acquisition section, which provides the estimates of the Doppler frequency and the code phase to the tracking section for more precise processing (Jiang et al., 2017). Consequently, to find the receiver PVT, the tracked navigational information and pseudo-ranges are sent to the navigation section. Although numerous methods have been proposed for improving the tracking and positioning sections (Li et al., 2014a; Teng and Wang, 2016; Guo et al., 2018; Teng et al., 2018; Ke et al., 2019), the acquisition of signals received from satellites is the first and the most important step in the software receiver (Liu et al., 2019b). Several methods can be utilised for the acquisition of the weak signals. These methods are classified into two general categories. The first category is called the serial search. Although this category cannot be used to create fast acquisition conditions, it is simple to implement it in hardware (Borio et al., 2008). The second category is the code phase search. It utilises fast Fourier transform (FFT) and inverse fast Fourier transform (IFFT) in the frequency domain to perform correlations across all pseudo-random noise (PRN) code phases at a given code and carrier Doppler frequency (Sagiraju et al., 2008). This category creates conditions for rapid acquisition, and it is used in most receivers (Chang et al., 2011; Li et al., 2014b). The FFT search method results from the circular cross-correlation in the time domain. Unlike the serial method which is required to step through different code phases and Doppler frequencies, the code phase search is only required to step through Doppler frequencies. Therefore, structures based on the FFT can be regarded as the fastest method for the acquisition of GPS signals (Kong, 2013).

Due to phenomena such as navigation bit sign transitions, code Doppler and residual Doppler frequency, these methods are not able to provide weak signal acquisition in low input signal-to-noise ratio (SNR) environments (Chung, 1995; Song et al., 2011). Several methods have been proposed for elimination of the bit sign transitions. Zhu and Fan (2015) proposed one method that employs a parallel algorithm and FFT method. Lin and Tsui (2001) introduced a half-bit method that was able to circumvent the effect of the navigation bits. The problem with this approach is that it only considers half of the navigation bit length while still suffering from squaring loss problems. Psiaki (2001) and Ziedan and Garrison (2004) also presented methods named 'full bit' and 'circle' that were able to estimate where the navigation bit sign transition occurs, respectively. Likewise, these methods suffer from the same problems of squaring loss and computational complexity. Other methods utilised in this field are called post-correlation techniques. Coherent integration is one of the techniques used to increase the integration time. The navigation bit sign transitions and the residual carrier phase Doppler frequency are two constraints that prevent increasing the integration time in this method (Shin and Lee, 2003; Elders-Boll and Dettmar, 2004). In non-coherent integration methods, though the navigation bit sign transitions are eliminated as a problem, there is a new issue that occurs in the detector output due to squaring operations. This is called squaring loss (Weixiao et al., 2010; Zeng et al., 2015). Differential methods are some of the most popular methods used for increasing the integration time and the amount of out SNR in weak signal environments (Sun, 2010; Esteves et al., 2016).

The post-correlation methods are suggested to increase the integration time, but despite their advantages, they suffer from the code Doppler phenomenon. This phenomenon occurs when long integration times causes the correlation peaks between the local coarse/acquisition (C/A) codes and the received signals not to fall into the same code phase because of the shifts that occur. Therefore, it reduces the out SNR in the desired code phase and hence the detection probability (Guo et al., 2017). Several solutions have been suggested for this problem. One of the simplest ideas as presented by (Ziedan, 2006) performs the compensation by producing a local version of the C/A code adjusted to properly account for the actual Doppler frequency. Psiaki (2001) has offered the concept of interpolation to solve this problem. Also, Jiao et al. (2012) have performed the compensation operation based on the theory of time-shifts. But the high computational complexity of these methods can be considered as their main shortcoming. Yichao et al. (2016) have suggested a method for compensation of code Doppler which not only has a low computational complexity, but also a fairly good performance.

We present an improved method that is both able to solve the problem of the navigation bit sign transitions and the code Doppler phenomenon which occurs in differential methods in a large number of integration times. The result of simulations performed based on three data sets indicates that the amount of required input SNR to detect at least four satellites in the proposed method is $-48{\cdot}3$ dB, but in traditional differential and non-coherent methods are -20 dB and -9 dB, respectively.

The rest of this paper is organised as follows. Section 2 presents a model of the received signal in the receiver and also describes the syntax of signal acquisition in weak signal environments. In Section 3 the problems of the code Doppler phenomenon and the navigation bit sign transition in weak signal environments are discussed. Next, in Section 4, the usual acquisition structure and consequently the improved structure are introduced. In Section 5 the simulation results are presented. Finally, the conclusions will be presented in Section 6.

2. SIGNAL MODEL AND ACQUISITION OPERATION IN WEAK SIGNAL ENVIRONMENTS.

The GPS signal will be taken to describe the proposed acquisition algorithm. Without loss of generality, it can be adopted in other navigation systems as well. GPS L1 C/A signal is binary phase shift keying (BPSK) modulated by a 50 bits per second (bps) navigation data stream and C/A code with a chip rate of $1{\cdot}023$ MHz. Each GPS satellite is allocated a unique PRN code to identify itself.

2.1. *Signal model.*

The GPS signals that are in the L1 band will be mixed to the IF band after they are received by the receiver. The received signals after the front-end can be displayed as follows:

$$r_{\mathrm{IF},i}(nT_s) = \sqrt{P_i}D_i(nT_s)c_i(nT_s - \tau_i + \zeta_i nT_s)\exp(j\,2\pi(f_{\mathrm{If}} + f_{d,i})nT_s + \varphi_{0,i}) + W(nT_s) \tag{1}$$

where $r_{\mathrm{IF},i}(nT_s)$ indicates the signal received from the i-th satellite, P_i is the power of the i-th satellite, $D_i(nT_s)$ is the indicator of the navigation data of the i-th satellite, T_s is the sampling time, $c_i(nT_s)$ is the C/A code of the i-th satellite, and τ_i indicates the code phase delay of the i-th satellite. f_{IF} shows the frequency of the IF band, and $f_{d,i}$ represents the Doppler frequency of the i-th satellite, which is produced due to the relative motion between the satellite and the receiver. $\zeta_i = f_{d,i} \cdot f_{\mathrm{chip}}/f_{\mathrm{RF}}$ represents the code-frequency offset of the i-th satellite, in which f_{chip} and f_{RF} denote the C/A code frequency and the carrier frequency, respectively. $\varphi_{0,i}$ models the initial phase of the i-th satellite and $W(n)$ specifies the Gaussian noise with zero mean and σ_n^2 variance.

https://doi.org/10.1017/S0373463320000028 Published online by Cambridge University Press

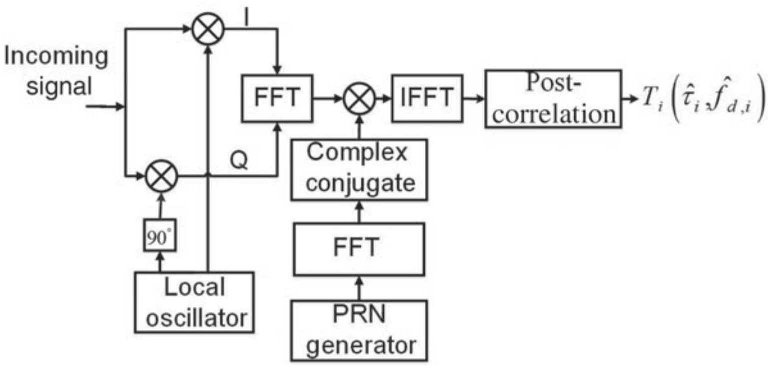

Figure 1. Acquisition structure in weak signal conditions.

2.1.1. *Acquisition operation in weak signal environments.* The acquisition operation in weak signal environments is usually based on the correlation between the incoming and local signals. This correlation can be defined as follows:

$$Z(\hat{\tau}_i,\hat{f}_{d,i}) = \sum_{n=0}^{N-1} r_{\mathrm{IF},i}(nT_s)c_i(nT_s - \hat{\tau}_i)\exp(-j\,2\pi\hat{f}_{d,i}nT_s) \tag{2}$$

where $Z(\hat{\tau}_i,\hat{f}_{d,i})$ denotes the correlation function or so-called ambiguity function. $\hat{\tau}_i$ and $\hat{f}_{d,i}$ are the estimates of the code phase and the Doppler frequency of the *i*-th satellite, respectively. N represents the number of samples (or code phases) in a C/A code period (usually one millisecond). After Equation (2) is estimated for the *i*-th satellite, the magnitude of $Z(\hat{\tau}_i,\hat{f}_{d,i})$ is compared with a predetermined threshold, and if it exceeds the threshold value, it shows that the *i*-th satellite is acquired and the code phase and the Doppler frequency estimates $(\hat{\tau}_i,\hat{f}_{d,i})$ will be delivered to the tracking section.

Since performing a correlation operation for a single C/A code period is inadequate in weak signal environments, the integration time must be increased. Therefore, the post-correlation techniques can be utilised to increase the amount of SNR in the output of detector. In Figure 1, the overall structure of the acquisition in weak signal environments can be observed. As shown in Figure 1, the post-correlation techniques are used after the correlation operation. These techniques can be divided into three categories (Parkinson et al., 1996; Sun, 2010): (1) coherent integration, (2) non-coherent integration, and (3) differential integration.

Each of these methods can be placed in the specified box of Figure 1. The coherent integration method has the following relationship:

$$T_i(\hat{\tau}_i,\hat{f}_{d,i}) = \left|\sum_{K=1}^{M} Z_K(\hat{\tau}_i,\hat{f}_{d,i})\right|^2 \tag{3}$$

where M represents the number of performed correlations. The effect of the residual carrier phase as well as the phenomenon of the navigation bit sign transition leads to a decrease in

https://doi.org/10.1017/S0373463320000028 Published online by Cambridge University Press

the output SNR. The non-coherent integration method can be expressed as follows:

$$T_i(\hat{\tau}_i, \hat{f}_{d,i}) = \sum_{K=1}^{M} \left| Z_K(\hat{\tau}_i, \hat{f}_{d,i}) \right|^2 \tag{4}$$

Although this method does not suffer from the same problems as the coherent integration, the square loss problem occurs in this method because of the squaring operation. In fact, this operation, in addition to boosting the ambiguity function peak, amplifies the amount of noise in the output of the detector. Also, Van Diggelen (2009) has shown that the combination of longer coherent and non-coherent integration is a powerful tool that can dramatically increase receiver sensitivity.

The differential method is the third method used in the post-correlation. Since the differential operation is performed in this method, some of the problems of the earlier methods are solved. When the correlation operation is accomplished, and the correlation outputs are generated, they will have almost the same phase. Therefore, since the noises of the correlation outputs are almost independent of each other, the output noises will be lost as a result of the differential operation. Various structures have been proposed for the differential method. These structures depend on how the correlation outputs are combined, and they can be categorised along with their decision variables as follows:

1. Coherent differential integration (Jeong et al., 2000):

$$T_i(\hat{\tau}_i, \hat{f}_{d,i}) = \left| \sum_{K=2}^{M} Z_K(\hat{\tau}_i, \hat{f}_{d,i}) Z_{K-1}^*(\hat{\tau}_i, \hat{f}_{d,i}) \right|^2 \tag{5}$$

2. Non-coherent differential integration (Pulikkoonattu and Antweiler, 2004):

$$T_i(\hat{\tau}_i, \hat{f}_{d,i}) = \sum_{K=2}^{M} \left| Z_K(\hat{\tau}_i, \hat{f}_{d,i}) Z_{K-1}^*(\hat{\tau}_i, \hat{f}_{d,i}) \right|^2 \tag{6}$$

3. Pair-wise coherent differential integration (Sun and Presti, 2010):

$$T_i(\hat{\tau}_i, \hat{f}_{d,i}) = \sum_{K=1}^{M/2} \left| Z_{2K}(\hat{\tau}_i, \hat{f}_{d,i}) Z_{2K-1}^*(\hat{\tau}_i, \hat{f}_{d,i}) \right|^2 \tag{7}$$

4. Pair-wise non-coherent differential integration (Sun and Presti, 2010):

$$T_i(\hat{\tau}_i, \hat{f}_{d,i}) = \sum_{K=1}^{M/2} \left| Z_{2K}(\hat{\tau}_i, \hat{f}_{d,i}) Z_{2K-1}^*(\hat{\tau}_i, \hat{f}_{d,i}) \right|^2 \tag{8}$$

5. Real differential integration (Zarrabizadeh and Sousa, 1997):

$$T_i(\hat{\tau}_i, \hat{f}_{d,i}) = \sum_{K=2}^{M} \mathrm{Re} \left\{ Z_K(\hat{\tau}_i, \hat{f}_{d,i}) Z_{K-1}^*(\hat{\tau}_i, \hat{f}_{d,i}) \right\}^2 \tag{9}$$

where Z_{K-1}^* represents the complex conjugate of Z_{K-1}. Zeng et al. (2015) compared different structures and proved that coherent differential integration has better results in comparison with other differential structures and post-correlation methods. Therefore, this method has been utilised in our improved structure.

https://doi.org/10.1017/S0373463320000028 Published online by Cambridge University Press

3. PROBLEMS OF POST-CORRELATION TECHNIQUES. Because of reduction of the output SNR by the navigation bit sign transitions and code Doppler, these are recognised as the main problems of the post-correlation techniques. The effect of the code Doppler gives rise to slipping the code chip during the correlation process. Navigation bit sign transitions can also cause a major problem for the acquisition performance. In this section, these issues will be completely reviewed.

3.1. *Problem of the navigation bit sign transition.* The problem of the navigation bit sign transition may occur in two conditions: (1) in the correlation between the local C/A code and the received signal, and (2) in performing the accumulation operation in the post-correlation techniques. In the first condition, the amount of output SNR reduction depends on the position of the bit sign transition within the correlation period. If it occurs in the middle of the C/A code period, the correlation is ideally zero (Van Diggelen, 2009; Xiang-Li and Jun, 2017). In the second condition, to increase the amount of output SNR, the number of accumulations will be increased. Since the length of each navigation bit is 20 ms, this phenomenon occurs at most once every 20 ms. If we assume that the bit sign transition occurs at exactly 10 ms, it causes the peak generated by the accumulation operation between the local C/A code and different 1 ms intervals of the received signal to be almost zero (Presti et al., 2009; Sun and Presti, 2010).

3.1.1. *Problem of the code Doppler.* The acquisition of satellite signals in GPS receivers is based on the correlation between the local C/A code and the received signal. As stated earlier, FFT is used to calculate Equation (2) for all points in the search space quickly. The FFT of the received signal and the local C/A code (this sampling assumes the nominal chipping rate of 1·023 MHz) can be shown as follows (Yichao et al., 2016):

$$C_i(k) = \mathrm{FFT}(c_i(nT_s)) \tag{10}$$

$$R_{i,\hat{f}_d}(k) = \mathrm{FFT}(r_{\mathrm{IF},i}(nT_s)\exp(-j\,2\pi\hat{f}_{d,i}nT_s)) \tag{11}$$

where $k = 0, 1, \ldots, N-1$, and $R_{i,\hat{f}_d}(k)$ denotes the FFT of the received signal of the i-th satellite in the d-th Doppler frequency, and $C_i(k)$ shows the FFT of the C/A code of the i-th satellite. Thus, the correlation between the received signal and the local C/A code of the i-th satellite in the d-th Doppler frequency can be shown as follows:

$$Z(\hat{\tau}_i, \hat{f}_{d,i}) = \mathrm{IFFT}(C_i^*(k)R_{i,\hat{f}_d}(k)) \tag{12}$$

In the above equation, IFFT represents the inverse FFT, so we will have:

$$Z(\hat{\tau}_i, \hat{f}_{d,i}) = \mathrm{IFFT}(C_i^*(k)R_{i,\hat{f}_d}(k)) = A_i(\Delta\tau)\mathrm{sinc}(\Delta\hat{f}_{d,i}T_c)\exp(\psi_{\mathrm{residual}}) \tag{13}$$

where T_c is the correlation time. $\Delta\hat{f}_{d,i} = f_{\mathrm{IF}} + f_{d,i} - \hat{f}_{d,i}$ denotes the remaining Doppler frequency of the i-th satellite. $A_i(\Delta\tau)$ indicates the C/A code self-correlation function of the i-th satellite, and ψ_{residual} is an indicator of the remaining carrier phase. Suppose that we want to find the K-th correlation between the received signal and the local C/A code of the i-th satellite in the d-th Doppler frequency, then we will have:

$$|Z_k(\hat{\tau}_i, \hat{f}_{d,i})| = |A_i(\tau - \hat{\tau}_i - \zeta_d KT_c)\mathrm{sinc}(\Delta\hat{f}_{d,i}T_c)| \tag{14}$$

In the above equation, $\xi_d KT_c$ is known as the linear code phase drift. Among the various correlations which take place between the C/A code and the received signal, this drift

https://doi.org/10.1017/S0373463320000028 Published online by Cambridge University Press

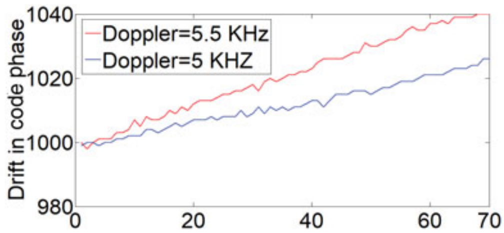

Figure 2. Shifts of maximum peaks due to the code Doppler phenomenon in PRN 1.

causes the code phase which places the highest correlation peak value to occur in different situations. In other words, instead of generating the correlation peak for satellite detection in a single code phase during different correlations, it will be distributed among several code phases, and it will be called the code Doppler phenomenon. The main effects of the code Doppler phenomenon are: (1) reducing the amplitude of the correlation function, and (2) shifting the real code phase.

Both of these cases cause reduction in the probability of detection. Therefore, they demonstrate the importance of compensation for this phenomenon. As indicated by the linear code phase drift equation, this phenomenon occurs due to the vast number of correlations (depending on the code-frequency offset and duration of integration). For further explanation, one GPS satellite with PRN 1 has been simulated in the L1 band, in which the number of correlations between the local C/A code and the received signal is M = 70 and the duration of each correlation one C/A code period (1 ms). The GPS signal used to simulate Figure 2 has the following information: (1) sampling frequency 5·1743 MHz, (2) C/A code frequency 1·023 MHz, and (3) C/A code length 1023.

In this simulation, satellite 1 has been utilised to illustrate the effect of code Doppler. Regarding the sampling frequency, there are 5,714 samples (code phases) in every C/A code period. In other words, there are nearly six samples in each chip. The effect of code Doppler is on the code phases of a PRN, not on its chips. That is why we have tried to use the code phase in the vertical axes to demonstrate this effect. In other words, when the number of correlations increases, the code phase which has the highest value of correlation is first shifted between the code phases of a chip and if the number of correlations is increased again, then it is entered into another chip. The result of this simulation is presented in Figure 2. According to Figure 2, increasing the number of correlations leads to shifting the code phase in which the correlation peak occurs, and the average of the shifts will be almost ascending.

4. PROPOSED METHOD.

As it was stated in the previous section, the problems of the post-correlation techniques are the code Doppler and the navigation bit sign transitions. Several solutions have been introduced by different researchers to compensate for these issues (Xiang-Li and Jun, 2017). Yichao et al. (2016) also suggested a solution that is efficient and produces more acceptable results compared with other code Doppler compensation techniques. Now, inspired by these solutions, we present our proposed structure in Figure 3. In this method, in addition to covering the weaknesses of the post-correlation techniques, computational complexity has also been avoided.

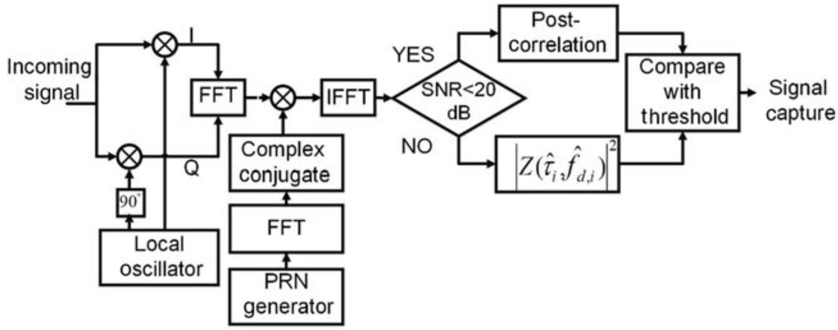

Figure 3. Structure of the improved semi-bit differential integration technique for compensation of the code Doppler phenomenon and the navigation bit sign transition.

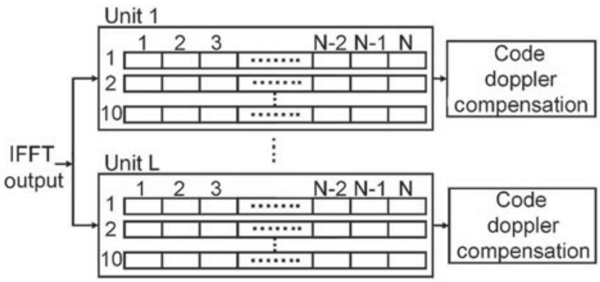

Figure 4. Post-correlation structure of the improved semi-bit differential integration technique for compensation of the code Doppler and any bit transitions.

In a weak signal environment, the received signals have low input SNR. Therefore, it is necessary to apply techniques that can increase the input SNR, but sometimes the received signals in this environment already have a high input SNR. In other words, it is possible that the GPS receiver exits the weak signal area for a moment. Thus, performing the post-correlation techniques will not be necessary. For this reason, we have utilised an SNR threshold of 20 dB in the proposed structure, in which the received signal is only sent for post-correlation processing if the input SNR is below this threshold value.

Figure 4 illustrates the structure that we have considered for the post-correlation operational unit. As it shows, this structure is divided into L units, in which each unit has ten 1 ms correlations between the received signal and the local C/A code (M = 10). The main reason for employing ten 1 ms correlations in each unit is to cope with navigation bit transitions. Due to the fact that each navigation bit takes as long as 20 ms, there would be some odd or even units in which the navigation bit transitions will not occur. For instance, if we suppose that L is equal to four, then the cases which may give rise to the navigation bit sign transition are shown in Figure 5. In Figure 4, to construct unit 1, 1 ms of the received signal is correlated with a period of the C/A code local signal based on Equation (2). The FFT has also been utilised to make this operation faster. The IFFT is then taken from the obtained result. Finally, it is regarded as a row in unit 1. This operation is repeated again for another millisecond of the input data to form the second row in unit 1. It is then performed continuously in the same way to create ten rows of unit 1. This procedure is also repeated

https://doi.org/10.1017/S0373463320000028 Published online by Cambridge University Press

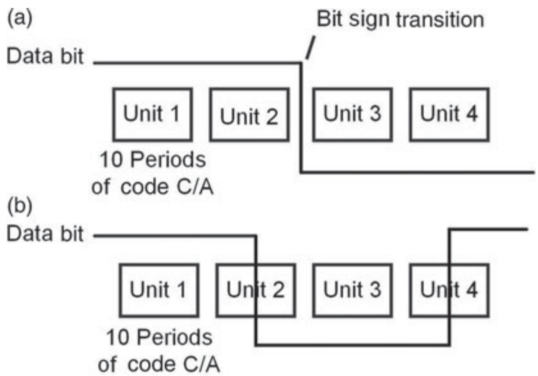

Figure 5. Cases in which the navigation bit may change.

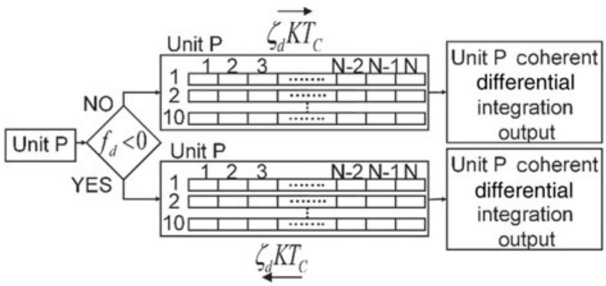

Figure 6. P-th sample of the code Doppler compensation block.

to construct units 2 to L. In fact, the difference between unit 1 and unit 2 is that the first and second 10 ms of the received signal are utilised for forming them, respectively. Similarly, other 10 ms intervals of the received signal are used to create units 3 to L. Notice that in Figure 4, N represents the number of samples (or code phases) in a C/A code period. In other words, it depends on the sampling time (T_s). For example, given that the sampling frequency is 5·7143 MHz, there are 5714 samples (code phases) in every C/A code period.

After this step, the computed correlations of all units are sent to the code Doppler compensation blocks. Figure 6 shows the p-th sample of the code Doppler compensation block. As shown in Figure 6, when the output of the p-th unit enters the related code Doppler compensation block, first it is checked whether the Doppler frequency is positive or negative. Then, if it is negative, the entire correlation function between the received signal and the local C/A code is shifted circularly based on Equation (13). Otherwise, it is vice versa. For further explanation, Equation (13) has three important parts where $\zeta_d = f_d \cdot f_{\text{chip}}/f_{\text{RF}}$ represents the code-frequency offset, T_c is the time of the correlation (here, it is considered as one of the C/A code periods), and K indicates the correlation number. This compensation is carried out for each correlation within every unit. In other words, $\xi_d KT_c$ represents the value of shifting the code phases of each correlation within every unit. After calculation $\xi_d KT_c$, its rounded value is utilised for the code Doppler compensation.

After the code Doppler compensation for all units, the correlation values of each unit are transmitted to the related block for differential integration. The integration operation is accomplished for the correlation values of each unit separately based on Equation (5).

https://doi.org/10.1017/S0373463320000028 Published online by Cambridge University Press

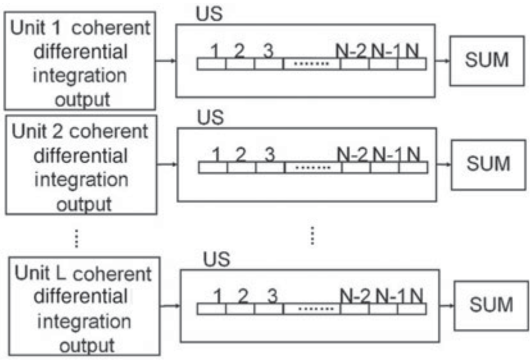

Figure 7. Performing unify sign (US) operation.

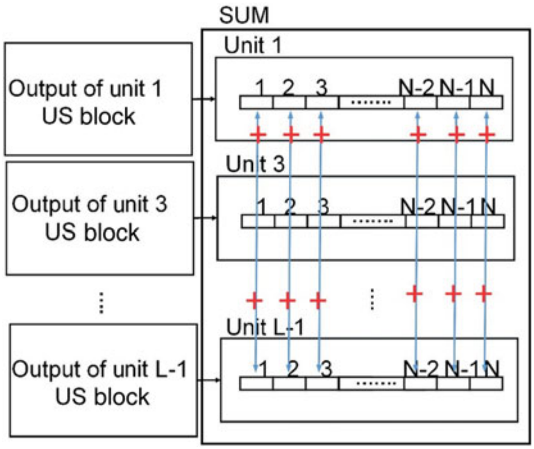

Figure 8. Sum operation of odd units.

In the next step, as shown in Figure 7, the coherent differential integration outputs of the units enter into a block called unify sign (US). The reason for the utilisation of this block is to equalise the output sign of odd and even units separately. For further explanation, see Figure 5. As can be seen, in the case of occurrence of the navigation bit sign transition, the odd or even units that have not experienced the change in the sign are affected by the opposite sign of the navigation bit. Therefore, it is necessary to solve this problem before adding the units. For the US operation, after performing the differential operation for all of the units, the outputs of differential blocks are as in Figure 7.

To equalise the signs, the real and imaginary values in each of code phases of unit 1 are individually compared and equalised with the real and imaginary values in the code phases of other odd units. Similarly, this US operation is carried out for unit 2 with other even units. After the US operation, the odd and even units are added together separately (it is assumed that L is an even number). To find the sum of odd units, their code phases are added as in Figure 8. Similarly, the sum of even units is performed.

As Figure 9 shows, after the sum of odd and even units, they are compared together, and the maximum value is considered to be compared with the predefined threshold. If the

https://doi.org/10.1017/S0373463320000028 Published online by Cambridge University Press

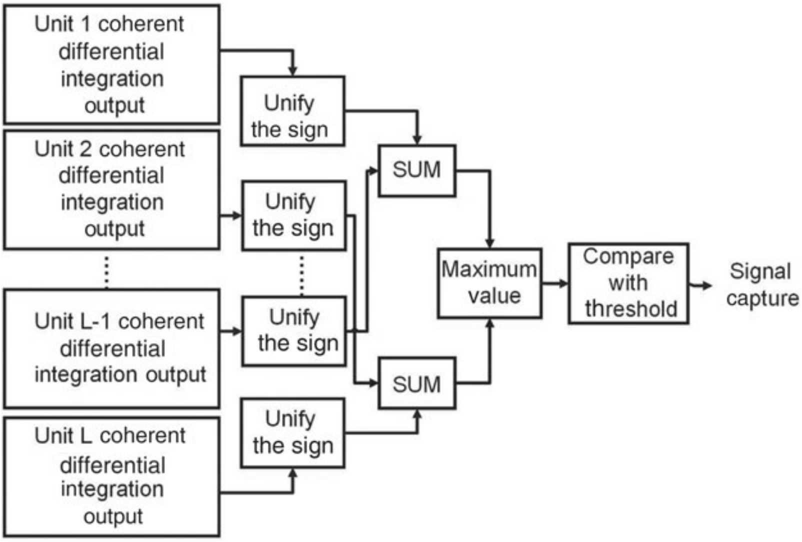

Figure 9. Last step of the proposed method.

Figure 10. Setup for recording real data around Iran University of Science and Technology.

result is greater than the threshold, the estimated code phase and the Doppler frequency are obtained and sent to the tracking section. Finally, we should notice that no pilot signals from other GNSS are supposed to exist when the proposed method is accomplished in the acquisition part of the receiver.

https://doi.org/10.1017/S0373463320000028 Published online by Cambridge University Press

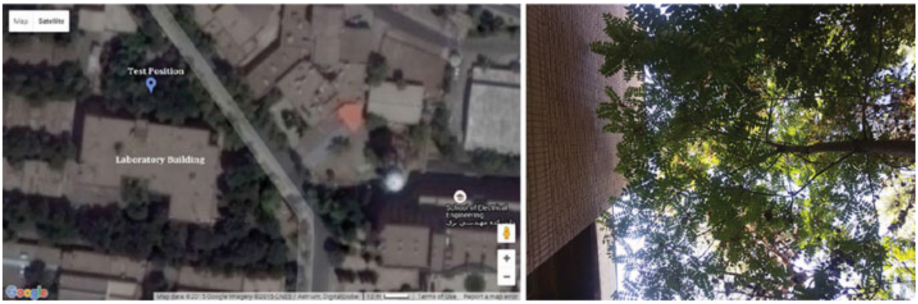

Figure 11. Recording real data in front of the IUST School of Electrical Engineering laboratory building where the view to the sky is blocked by buildings and trees.

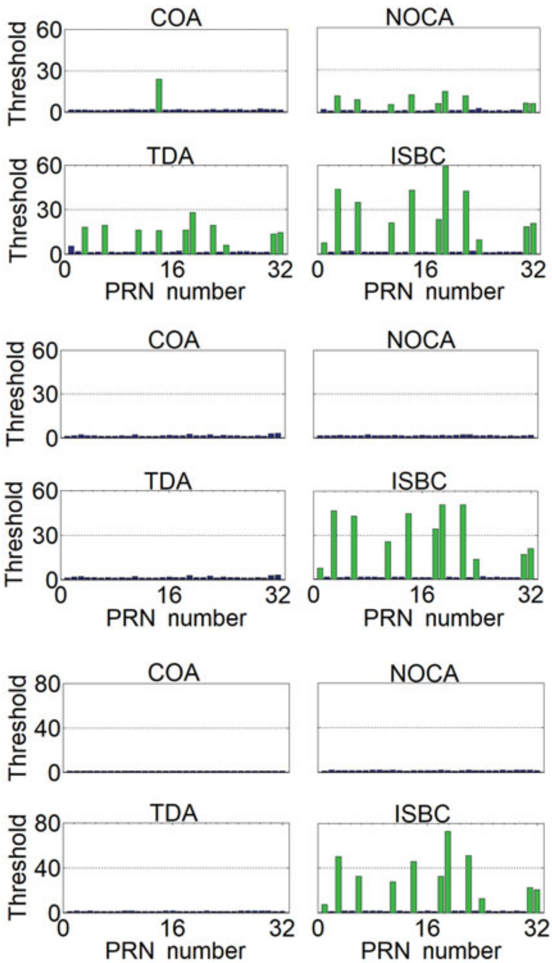

Figure 12. Peak value and detection status for each satellite search in NOCA, COA, TDA and ISBC methods for $M = 20$, $T = 1$ ms, input SNR = 13·3 dB (top), $M = 40$, $T = 1$ ms, input SNR = 13·3 dB (middle) and $M = 80$, $T = 1$ ms, input SNR = 13·3 dB (bottom). (Not acquired signals (black), acquired signals (green))

https://doi.org/10.1017/S0373463320000028 Published online by Cambridge University Press

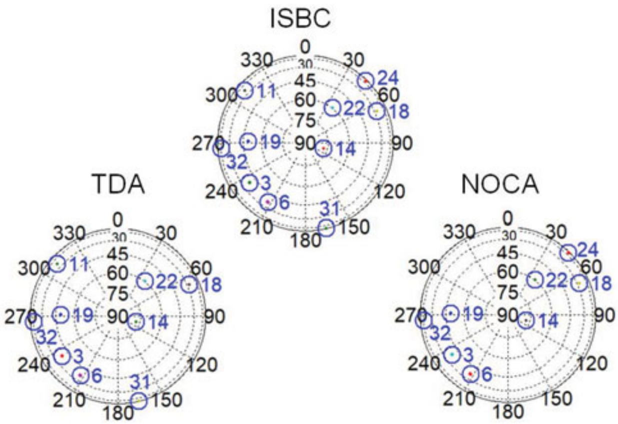

Figure 13. Sky plots of methods for $M = 20$ and $T = 1$ ms.

Table 1. The results of acquisition for $M = 20$, and $T = 1$ ms.

Methods	Input SNR (dB)	Output SNR (dB)	Maximum peak	Number of acquired satellites	CPU time (s)
COA	13·3	19·1	24	1	82
NOCA	13·3	29·8	15	8	108
TDA	13·3	37·1	28	9	115
ISBC	13·3	56	59	10	130

5. PERFORMANCE ANALYSIS. The improved semi-bit compensation (ISBC) method is simulated and compared with three alternative methods: (1) coherent accumulation (COA), (2) non-coherent accumulation (NOCA), and (3) traditional differential accumulation (TDA).

In this study, we have utilised three data sets. The first data set is related to real data which was recorded from the streets around Iran University of Science and Technology (IUST). The process of recording the data is presented in Figure 10. The characteristics of the first data set are as follows. The C/A code is a gold sequence with a length of 1023 chips. The carrier frequency of the received signal is 1575·42 MHz. The maximum Doppler carrier-frequency range is 20 KHz. The intermediate frequency of the acquisition stage is 4·309 MHz, and the location of the code phase in the signal and the existence of bit transitions are random. The sampling rate is set at 5·7143 MHz. The second data set is also real data which was recorded in front of the IUST School of Electrical Engineering laboratory building where the view to the sky is blocked by buildings and trees (Figure 11). The third data set is related to the simulation data of the static user. It was collected by the multi-GNSS constellation simulator from Spirent. The characteristics of the second and third data sets are the same as the first one. Note that although various techniques have been accomplished to meet the requirements of GPS indoors (Liu et al., 2018; Liu et al., 2019a), as Figures 10 and 11 show, the scenarios considered here for the results of the proposed ISBC method and the traditional methods are concerned with the characteristics of urban areas such as tall buildings, trees, and etc.

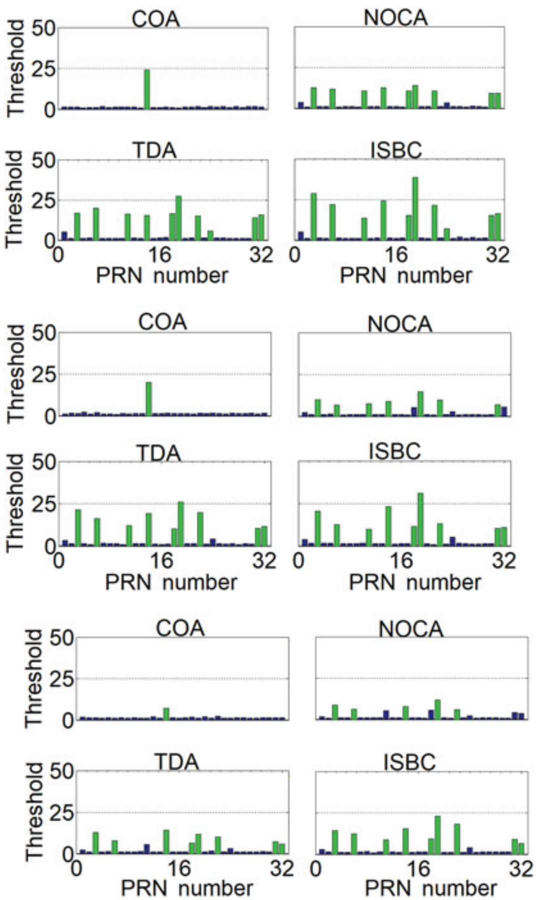

Figure 14. Peak value and detection status for each satellite search in NOCA, COA, TDA and ISBC methods for $M = 20$, $T = 1$ ms, input SNR = 10 dB (top), $M = 20$, $T = 1$ ms, input $SNR = 7$ dB (middle) and $M = 20$, $T = 1$ ms, input $SNR = 2$ dB (bottom). (Not acquired signals (black), acquired signals (green)).

To compare the proposed structure with other methods, first, the number of acquired satellites and the peak value for each of the above methods are obtained. Second, to create the weak signal, noise is added and the previous operation is repeated. Finally, the SNR gain for each method is calculated.

5.1. *Simulation results.* The first part of the simulation, concerned with the second data set which was recorded in front of the IUST School of Electrical Engineering laboratory building where the view to the sky is blocked by buildings and trees (a weak signal environment), is to find the number of acquired satellites and the maximum peak value for comparing different amounts of accumulation with the threshold. Figure 12 shows the results of this part. It is clear that, as the number of correlations (M) between the local C/A code and the received signal increases, as a result of the occurrence of the navigation bit sign transitions and the code Doppler, the amount of the output peaks and the number of acquired satellites decreases. But in our proposed method, by increasing the number of correlations, not only do the peak values improve but also the number of acquired satellites

https://doi.org/10.1017/S0373463320000028 Published online by Cambridge University Press

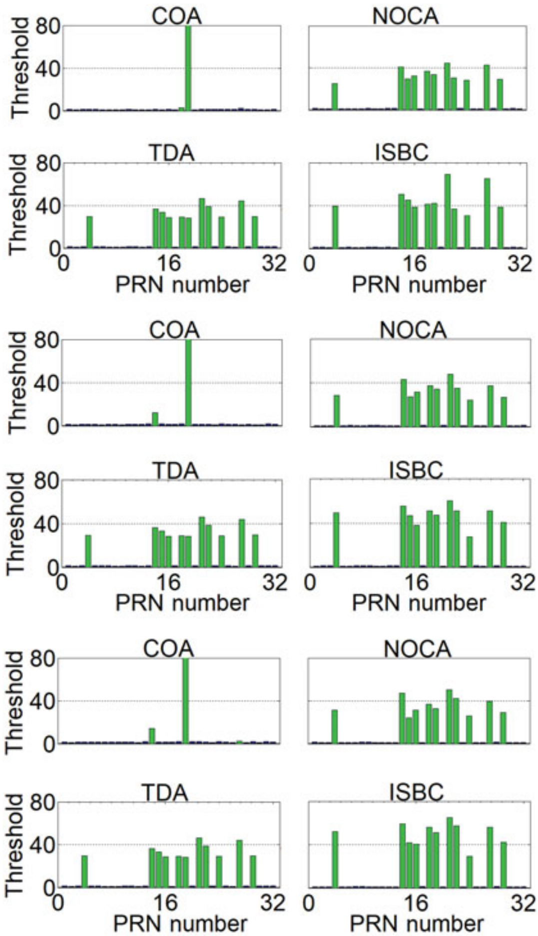

Figure 15. Peak value and detection status for each satellite search in NOCA, COA, TDA and ISBC methods in the first dataset for M = 20, T = 1 ms (top), M = 40, T = 1 ms (middle) and M = 80, T = 1 ms (bottom). (Not acquired signals (black), Acquired signals (green)).

does not diminish. Figure 13 indicates the sky plots of the methods for M = 20. Table 1 shows the results of acquisition for M = 20 and T = 1 ms, input SNR = 13·3 dB.

In order to validate the proposed method under different input SNRs in the second data set, the white Gaussian noise (WGN) function in MATLAB is utilised to achieve weaker signals. So, the various kinds of Gaussian noise with different powers are produced and combined with the main signal. The simulation results are presented in Figure 14. As shown, the peaks of satellites in the proposed method are more than other methods when input SNR decreases.

In the second part of the simulation, two other data sets were simulated to demonstrate that the proposed method is independent of the receiver input data. The results of the first data set, which was recorded from the streets around IUST, and the third data set which is related to the simulation data of the static user are presented in Figures 15 and 16,

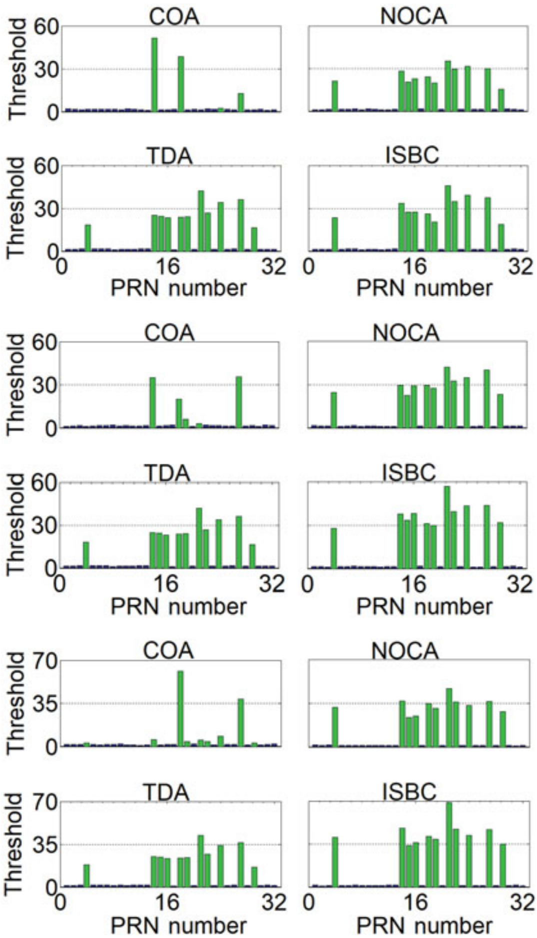

Figure 16. Peak value and detection status for each satellite search in NOCA, COA, TDA and ISBC methods in the third dataset for $M = 20$, $T = 1$ ms (top), $M = 40$, $T = 1$ ms (middle) and $M = 80$, $T = 1$ ms (bottom). (Not acquired signals (black), acquired signals (green)).

respectively. As shown, the ISBC method is not only independent of the type of input data but also outperforms compared with the traditional method.

Finally, to evaluate the proposed method in the worst case, various kinds of Gaussian noise with different powers were produced using the WGN function and combined with the main signals in the second data set. Figure 17 shows the comparison between traditional methods and the proposed method based on input SNR, and the SNR gain, which is defined as follows:

$$\text{SNRGain} = \frac{\text{OutputSNR}}{\text{InputSNR}} \tag{15}$$

According to Figure 17, the amount of required input SNR to detect at least four satellites in the ISBC method is $-48{\cdot}3$ dB, but in the TDA and NOCA methods, they are -20 dB and -9 dB, respectively. Figure 18 also shows the results of detecting at least four satellites for the mentioned methods.

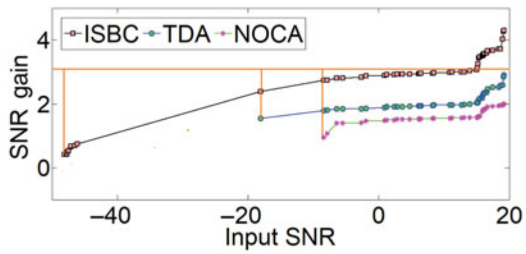

Figure 17. Comparison between traditional methods and the proposed method based on SNR gain.

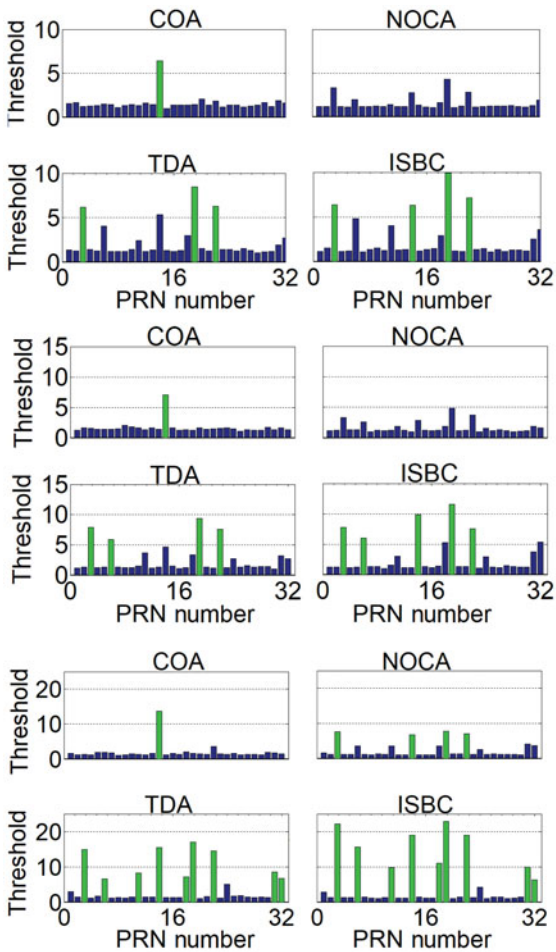

Figure 18. Peak values and the minimum amount of required input SNR to detect at least four satellites for ISBC, $M = 20$, $T = 1$ ms, input SNR = −48·3 dB (top), TDA, $M = 20$, $T = 1$ ms, input SNR = −20 dB (middle) and NOCA, $M = 20$, $T = 1$ ms, input SNR = −9 dB (bottom). (Not acquired signals (black), acquired signals (green)).

https://doi.org/10.1017/S0373463320000028 Published online by Cambridge University Press

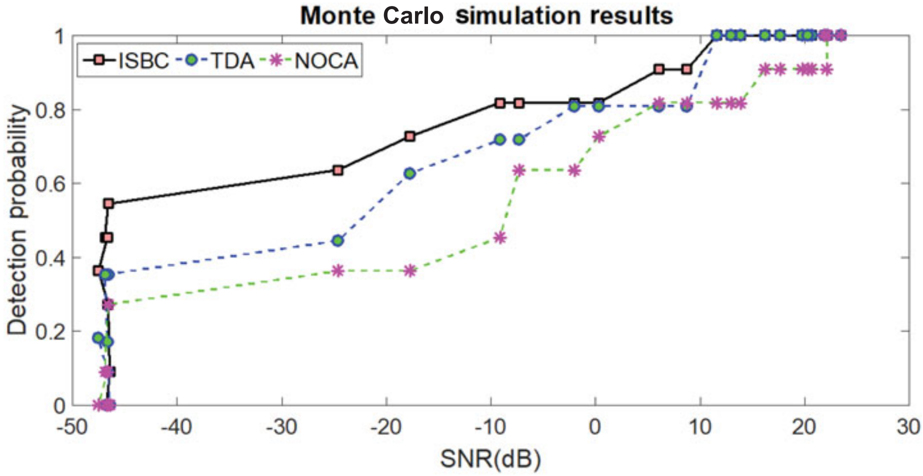

Figure 19. Detection probability of the different methods with the false detection probability being 1e-6 under coherent time being 1 ms.

In Figure 19, we give a comparison of the detection probability between the non-coherent integration, differential coherent integration, and the proposed method of ISBC with the false detection probability being 1e-6 and the coherent time of 1 ms under the second data set which has been recorded in front of the IUST School of Electrical Engineering laboratory building. As Figure 19 shows, the ISBC method is superior to the traditional methods.

6. CONCLUSION. The post-correlation techniques are utilised in weak signal environments to increase the amount of SNR in detector output. Although these methods have some advantages, they still suffer from the code Doppler and the navigation bit sign transition problems yet. The first problem shifts the real code phase that means the maximum peak of different correlations does not fall in the same code phase. The second problem decreases the amplitude of the correlation function. On the other hand, both of them reduce detection of satellites in the detector output. In the present study, an improved semi-bit differential acquisition method for the bit sign transition and the code Doppler compensation was addressed and examined on three available data sets. To eliminate the navigation bit sign transitions in the proposed method, 10 ms correlations were performed in the even and odd units individually due to the navigation bit flipping that occurs every 20 ms. Thus, the maximum pick of correlation results between the received signal and the local C/A code appears in one of integrated even and odd units. Moreover, in order to tackle the issue of linear code phase drift in weak signal environments, the presented method compensates the code Doppler for every correlation result by calculating the code-frequency offset. The results showed that the proposed method has better performance compared with the traditional methods in the input SNR required to detect at least four satellites.

REFERENCES

Borio, D., Camoriano, L. and Presti, L. L. (2008). Impact of GPS acquisition strategy on decision probabilities. *IEEE Transactions on Aerospace and Electronic Systems*, **44**(3), 996–1011.

Chang, L., Jun, Z., Zhu, Y. and Qingge, P. (2011) Analysis and Optimization of PMF-FFT Acquisition Algorithm for High-Dynamic GPS Signal. *IEEE 5th International Conference on Cybernetics and Intelligent Systems (CIS)*, Qingdao, China, September 17–19, 185–189.

Chung, C. D. (1995). Differentially coherent detection technique for direct-sequence code acquisition in a Rayleigh fading mobile channel. *IEEE Transactions on Communications*, **43**(234), 1116–1126.

Elders-Boll, H. and Dettmar, U. (2004). Efficient Differentially Coherent Code/Doppler Acquisition of Weak GPS Signals. *IEEE Eighth International Symposium on Spread Spectrum Techniques and Applications*, NSW, Australia, 30 August–2 September, 731–735.

Esteves, P., Sahmoudi, M. and Boucheret, M. L. (2016). Sensitivity characterization of differential detectors for acquisition of weak GNSS signals. *IEEE Transactions on Aerospace and Electronic Systems*, **52**(1), 20–37.

Guo, Y., Huan, H., Tao, R. and Wang, Y. (2017). Long-term integration based on two-stage differential acquisition for weak direct sequence spread spectrum signal. *IET Communications*, **11**(6), 878–886.

Guo, X., Zhou, Y., Wang, J., Liu, K. and Liu, C. (2018). Precise point positioning for ground-based navigation systems without accurate time synchronization. *GPS Solutions*, **22**(2), 34.

Jeong, Y. K., Lee, K. B. and Shin, O. S. (2000) Differentially Coherent Combining for Slot Synchronization in Inter-Cell Asynchronous DS/SS Systems. *The 11th IEEE International Symposium on Indoor and Mobile Radio Communications*, London, United Kingdom.

Jiang, R., Wang, K. and Wang, J. (2017). Performance analysis and design of the optimal frequency-ýassisted phase tracking loop. *GPS Solutions*, **21**(2), 759–768.

Jiao, X. P., Wang, J. and Li, X. (2012) High Sensitivity GPS Acquisition Algorithm Based on Code Doppler Compensation. *IEEE 11th International Conference on Signal Processing (ICSP)*, Beijing, China, 21–25 October, 241–245.

Kaplan, E. and Hegarty, C. (2005) *Understanding GPS: Principles and Applications*. Boston: Artech House.

Ke, F., Wang, J., Tu, M., Wang, X., Wang, X., Zhao, X. and Deng, J. (2019). Characteristics and coupling mechanism of GPS ionospheric scintillation responses to the tropical cyclones in Australia. *GPS Solutions*, **23**(2), 34.

Kong, S. H. (2013). A deterministic compressed GNSS acquisition technique. *IEEE Transactions on Vehicular Technology*, **62**(2), 511–521.

Li, T., Wang, J. and Laurichesse, D. (2014a). Modeling and quality control for reliable precise point positioning integer ambiguity resolution with GNSS modernization. *GPS Solutions*, **18**(3), 429–442.

Li, S., Yi, Q., Shi, M. and Chen, Q. (2014b) Highly Sensitive Weak Signal Acquisition Method for GPS/Compass. *International Joint Conference on Neural Networks (IJCNN)*, Beijing, China, 6–11 July, 1245–1249.

Lin, D. M. and Tsui, J. B. Y. (2001) A Software GPS Receiver for Weak Signals. *IEEE International Microwave Symposium Digest (MTT-S)*, Phoenix, USA, 20–24 May, 2139–2142.

Liu, Q., Huang, Z., Kou, Y. and Wang, J. (2018). A low-ambiguity signal waveform for pseudolite ýpositioning systems based on chirp. *Sensors (Switzerland)*, **18**(5), 1326.

Liu, Q., Huang, Z. and Wang, J. (2019a). Indoor non-line-of-sight and multipath detection using deep learning approach. *GPS Solutions*, **23**(3), 75.

Liu, Q., Kou, Y., Huang, Z., Wang, J. and Yao, Y. (2019b). Mean acquisition time analysis for GNSS ýparallel and hybrid search strategies. *GPS Solutions*, **23**(4), 94.

Parkinson, B. W., Enge, P., Axelrad, P. and Spilker, J. J. Jr (1996) *Global Positioning System: Theory and Applications*, Vol. II. Washington, USA: American Institute of Aeronautics and Astronautics.

Presti, L. L., Zhu, X., Fantino, M. and Mulassano, P. (2009). GNSS signal acquisition in the presence of sign transition. *IEEE Journal of Selected Topics in Signal Processing*, **3**(4), 557–570.

Psiaki, M. L. (2001) Block Acquisition of Weak GPS Signals in a Software Receiver. *Proceedings of ION GPS 2001, Institute of Navigation*, Salt Lake City, UT, 11–14 September, 2838–2850.

Pulikkoonattu, R. and Antweiler, M. (2004) Analysis of Differential Non Coherent Detection Scheme for CDMA Pseudo Random (PN) Code Acquisition. *IEEE International Symposium on Spread Spectrum Techniques and Applications*, NSW, Australia, 30 August–2 September, 212–217.

Sagiraju, P., Raju, G. and Akopian, D. (2008). Fast acquisition implementation for high sensitivity global positioning systems receivers based on joint and reduced space search. *IET Radar, Sonar & Navigation*, **2**(5), 376–387.

Shin, O. S. and Lee, K. B. (2003). Differentially coherent combining for double-dwell code acquisition in DS-CDMA systems. *IEEE Transactions on Communications*, **51**(7), 1046–1050.

Song, Y., Li, X., Yang, Y. and Liu, L. (2011) Enhanced Full Bit Acquisition Algorithm for Software GPS Receiver in Weak Signal Environment. *International Conference on Computational Problem-Solving (ICCP)*, Chengdu, China, 21–23 October, 440–443.

Sun, K. (2010) A Differential Strategy for GNSS Weak Signals Acquisition in Presence of Bit Sign Transitions. *6th International Conference on Wireless Communications Networking and Mobile Computing (WiCOM)*, Chengdu, China, 23–25 September, 1–5.

Sun, K. and Presti, L. L. (2010) A Differential Post Detection Technique for Two Steps GNSS Signal Acquisition Algorithm. *Proceedings of IEEE/ION PLANS 2010, Institute of Navigation*. Indian Wells, CA, 4–6 May, 752–764.

Teng, Y. and Wang, J. (2016). A closed-form formula to calculate geometric dilution of precision (GDOP) for multi-GNSS constellations. *GPS Solutions*, **20**(3), 331–339.

Teng, Y., Wang, J., Huang, Q. and Liu, B. (2018). New characteristics of weighted GDOP in multi-GNSS positioning. *GPS Solutions*, **22**(3), 74.

Van Diggelen, F. (2009) *A-GPS: Assisted GPS, GNSS, and SBAS*. London, UK/Norwood, MA, USA: Artech House.

Weixiao, M., Ruofei, M. and Shuai, H. (2010) Optimum Path Based Differential Coherent Integration Algorithm for GPS C/A Code Acquisition Under Weak Signal Environment. *First International Conference on Pervasive Computing Signal Processing and Applications (PCSPA)*, Harbin, China, 17–19 September, 1201–1204.

Xiang-Li, Z. and Jun, Y. (2017) Semi-bit Frequency Compensation Differential Combining Post-Correlation Processing for GNSS Weak Signal Environment. *2nd Asia-Pacific Conference on Intelligent Robot Systems (ACIRS)*, Wuhan, China, 16–18 June, 129–136.

Yichao, G., Jianmin, G., Pin, L., Hao, H. and Ran, T. (2016). A Code Doppler Compensation Algorithm in Acquisition for High Dynamic Spread Spectrum Signals. *IEEE International Conference on Signal Processing Communications and Computing (ICSPCC)*, Hong Kong, China, 5–8 August, 1–5.

Zarrabizadeh, M. H. and Sousa, E. S. (1997). A differentially coherent PN code acquisition receiver for CDMA systems. *IEEE Transactions on Communications*, **45**(11), 1456–1465.

Zeng, D., Ou, S., Li, J., Sun, J., Yan, Y. and Li, H. (2015). Analysis and Comparison of Non-coherent and Differential Acquisition Integration Strategies. In: Sun, J., Liu, J., Fan, S. and Lu, X. (eds.). *China Satellite Navigation Conference (CSNC) 2015 Proceedings: Volume I*. Lecture Notes in Electrical Engineering, vol. 340. Berlin, Heidelberg: Springer, 163–176.

Zhu, C. and Fan, X. (2015). A novel method to extend coherent integration for weak GPS signal acquisition. *IEEE Communications Letters*, **19**(8), 1343–1346.

Ziedan, N. I. (2006). *GNSS Receivers for Weak Signals*. Norwood, MA, USA: Artech House.

Ziedan, N. I. and Garrison, J. L. (2004) Unaided Acquisition of Weak GPS Signals Using Circular Correlation or Double-Block Zero Padding. In *Position Location and Navigation Symposium*, Monterey, USA, 26–29 April, 461–470.